Supplementary Material

Micro-nano bubbles enhanced degradation of emerging contaminants by ferrous-oxalate complexes: Synergistic interaction between oxidation and coagulation

Ping Li[1,2,#], Xiaojiang Huang[1,2,#], Qing Yang[3], Haozhe Xia[4], Chunbo Li[1,2], Zhiqiang Zhang[1,2], Xuan Wang[1,2], Jinsuo Lu (✉)[1,2]

1 School of Environmental and Municipal Engineering, Xi'an University of Architecture and Technology, Xi'an 710055, China

2 Key Laboratory of Northwest Water Resources, Environment and Ecology, Ministry of Education, Xi'an 710055, China

3 Ministry of Education Engineering Research Center of Water Resource Comprehensive Utilization in Cold and Arid Regions, Lanzhou 730070, China

4 Xi'an Municipal Water Supply Co., Xi'an 710055, China

Table S1 HPLC conditions for emerging contaminant analyses.

Compounds	Eluent ratio (%)			Flow rate	Wavelength
	methanol	acetonitrile	ultrapure water	(mL/min)	(nm)
BPS	50		50	1.0	260
SDZ	45		55	1.0	270
CBZ		50	50	1.0	280
ATZ		60	40	1.0	222
p-HBA	35		65	1.0	254
PMSO		30	70	1.0	230
$PMSO_2$		30	70	1.0	215

✉ Corresponding author
E-mail: lujinsuo@xauat.edu.cn
# Ping Li and Xiaojiang Huang contributed equally to this work.

Table S2 Identification of transformation products and structures in BPS degradation.

Product	Formula	Molecular molar mass	m/z value	Structure
BPS	$C_{12}H_{10}O_4S$	250.0300	249.0227	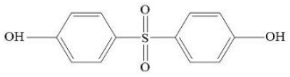
TP1	$C_{12}H_{10}O_5S$	266.0258	265.0179	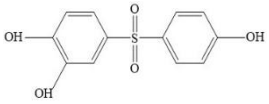
TP2	$C_{12}H_{10}O_6S$	282.0196	281.0123	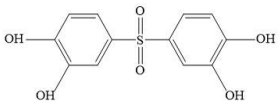
TP3	$C_{12}H_{26}O_4S$	266.1550	265.1475	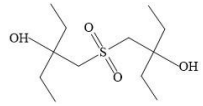
TP4	$C_{12}H_{10}O_4$	218.0565	217.0421	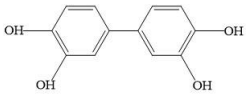
TP5	$C_{12}H_{18}O_2$	194.1315	193.1257	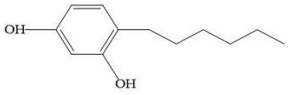
TP6	$C_{12}H_{20}O_3$	212.1408	211.1336	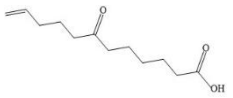
TP7	$C_6H_6O_4S$	173.9982	172.9913	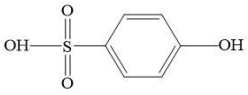
TP8	$C_7H_6O_5S$	201.9930	200.9856	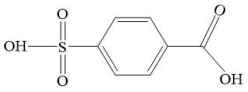
TP9	$C_7H_6O_4S$	185.9969	184.9903	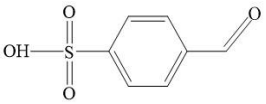
TP10	$C_7H_6O_2$	122.0366	121.0291	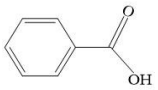
TP11	C_7H_6O	106.0408	105.0338	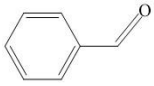
TP12	H_2O_4S	97.9672	96.9598	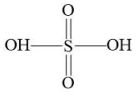

TP13	$C_6H_{10}O_4S$	178.0295	177.0158	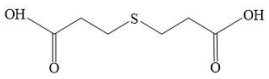
TP14	$C_6H_{10}O_2S$	146.0404	145.0349	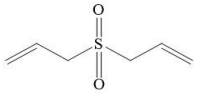
TP15	$C_6H_{14}O_4S$	182.0602	181.0575	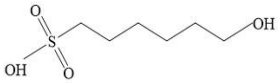
TP16	C_6H_6O	94.0415	93.0342	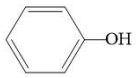
TP17	$C_6H_6O_6$	174.0181	173.0108	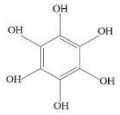
TP18	$C_6H_{10}O_4$	146.0565	145.0473	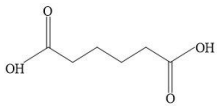
TP19	$C_6H_{10}O_5$	162.0537	161.0463	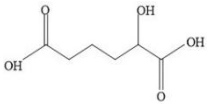
TP20	$C_6H_4O_2$	108.0212	107.0150	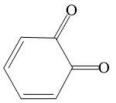

Text S1. BPS and $Na_2C_2O_4$ stock solution configuration

BPS stock solution: weighed 100 mg of BPS and dissolved it in 1000 mL of deionized water to form 100 mg/L BPS stock solution.

$Na_2C_2O_4$ stock solution: weighed 20 g of $Na_2C_2O_4$ dissolved in 1000 mL of deionized water, configured to 0.15 mmol/L $Na_2C_2O_4$ stock solution.

Text S2. Identification of degradation BPS intermediates by LC-MS

BPS transformation products were analyzed using an Agilent 1260 Infinity II Prime liquid mass spectrometer (Agilent 1260 Infinity II Prime, USA). The separation was performed on an InfinityLab Poroshell 120 EC-C18 column (3.0 mm × 100 mm). The gradient mobile phase consisted of 0.1% formic acid in water (phase A) and methanol (phase B). The injection volume was 5.0 μL, and the column temperature was 30℃. The elution program was as follows: 0 min10% B, 1 min10% B, 5 min 50% B, 10 min 85% B, 11 min 95% B, 15 min 95% B, 20 min 10% B, 23 min 10% B. The flow rate was 0.4 mL/min. All transformation products were characterized by ESI negative mode mass spectrometry scanning. Ion

source parameters were: ion source, ESI; warping gas rate, 30 mL/min; auxiliary gas rate, 5 mL/min; spray voltage, negative ion 2.8 kV; capillary temperature:300℃; scan mode: Fullms/dd-ms2 top10; scan range: primary scan: resolution 70000, range 100–1500 m/z; secondary scan: Resolution 17500, starting ion 50 m/z; fragmentation energy: HCD15, 30, 45.

Text S3. The test methods for the concentration of Fe^{2+} and Fe_{tot}

The concentrations of Fe^{2+} and total iron (Fe_{tot}) were determined using a UV-Vis spectrophotometer (U-3900, Hitachi, Japan). 10 mL of water sample was added to 50 mL of colorimetric tube containing 5 mL of acetic acid-ammonium acetate buffer solution, and then 2 mL of 0.5% 1,10-phenanthroline, and the absorbance was measured at λ = 510 nm after 10 min of color development. For Fe_{tot} measurement, 1 mL of 10% hydroxylamine hydrochloride was added before color development.

Text S4. Spectral characteristics and correlations with iron species

On the basis of the calculations, the linear differential absorbance (DA) method was applied to exhibit the process (Eq. (S1)):

$$DA_{\lambda} = A_{\lambda,i} - A_{\lambda,0} \quad , \quad (S1)$$

where $A_{\lambda,i}$ represented the absorbance at a specific wavelength after reaction period i, and $A_{\lambda,0}$ represented the absorbance before MNBs/Fe^{2+}/Ox treatment.

To identify the structure of the iron hydrolysis products in detail, the software Peakfit (version 4.12) was used to deconvolve the UV differential spectra, and the algorithm assumed that the absorption bands were Gaussian, and the corresponding photon energies were calculated as follows (Eq. (S2)):

$$E(eV) = \frac{1240}{\lambda(nm)} \quad , \quad (S2)$$

Each Gaussian spectrum (A_i) is characterized by peak height (E_{0i}), peak width (W_i), and amplitude (A_{0i}), and the spectra were calculated as follows (Eq. (S3)):

$$\Delta A(E) = \varepsilon \Delta A_i = \varepsilon \Delta A_{0i} \exp\left[-\frac{1}{2}\left(\frac{E-E_{0i}}{W_i}\right)^2\right] \quad , \quad (S3)$$

Running the program for simultaneous and iterative optimization of the positions of the absorption bands and absorbance values resulted in a good fit of the fitted spectra to the experimentally measured spectra ($R^2 > 0.99$). Since the wavelengths of the spectral peaks are not fixed but are determined by an algorithm to find the best spectral fit, the inverse plethysmographic product of random absorption spectra theoretically produces combinations of absorption bands with different peak wavelengths. The spectrum of iron hydrolysis products consisted of six Gaussian components in the range of 190–400 nm; which were 205 nm ($FeOH^{2+}$), 220 nm ($FeOH^{2+}$), 260 nm (Fe^{3+}), 300 nm ($Fe(OH)_2^{+}$), 335 nm ($Fe_2(OH)_2^{4+}$), and 372

nm ($Fe_3(OH)_4^{5+}$), respectively. $FeOH^{2+}$ represented mononuclear iron hydroxide and $Fe(OH)_2^{+}$, $Fe_2(OH)_2^{4+}$ and $Fe_3(OH)_4^{5+}$ represented polynuclear iron hydroxide.

Text S5. The test methods for the concentration of $O_2^{\bullet-}$

Nitroblue tetrazolium chloride (NBT) was used as the probe for the detection of superoxide radicals. The diformazan, which is the product of the reaction of NBT with $O_2^{\bullet-}$, has a strong absorption at 560 nm. During the experiment, a reaction of 4 mL of 10 mmol/L NBT stock solution, mixed with 5 mL of sample solution was reacted for 10 min, followed by measurements. The concentration of $O_2^{\bullet-}$ was qualitatively analyzed by absorbance.

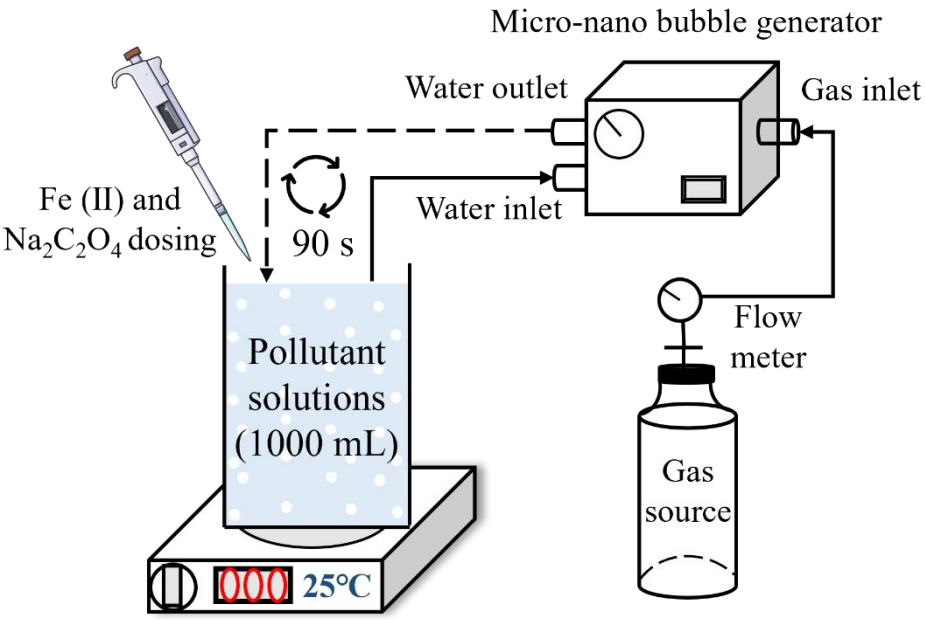

Fig. S1 Device model of MNBs/Fe^{2+}/Ox system.

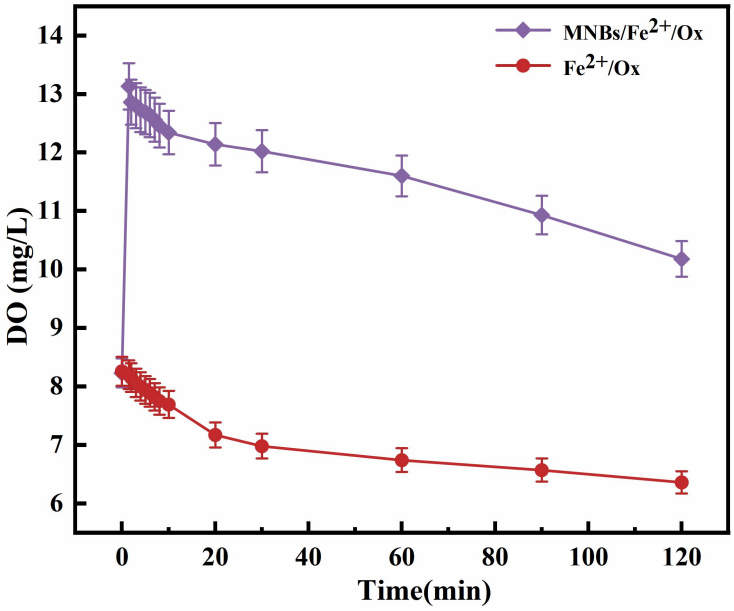

Fig. S2 Changes of DO concentration in the system with and without MNBs participation. (pH = 7.0, [Fe^{2+}] = 0.1 mmol/L, [oxalate] = 0.5 mmol/L, BPS = 100 μg/L, Q_g = 10 mL/min, t = 90 s).

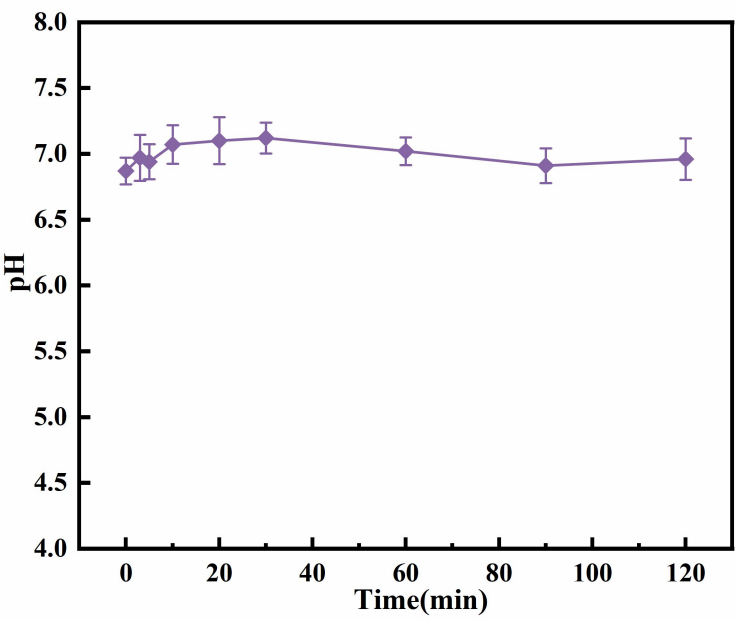

Fig. S3 Changes of pH value during the reaction in MNBs/Fe^{2+}/Ox system. ([Fe^{2+}] = 0.1 mmol/L, [oxalate] = 0.5 mmol/L, BPS = 100 μg/L, Q_g = 10 mL/min, t = 90 s).

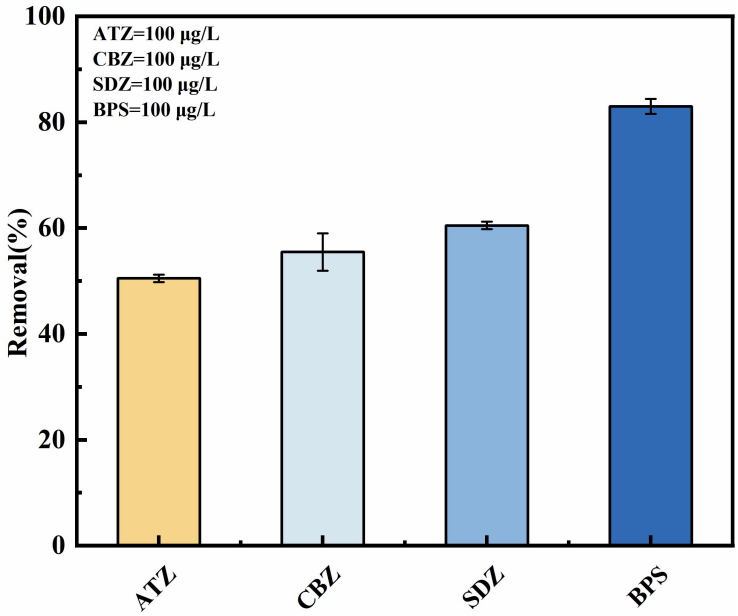

Fig. S4 Removal of different contaminants by MNBs/Fe^{2+}/Ox system. (pH = 7.0, [Fe^{2+}] = 0.1 mmol/L, [oxalate] = 0.5 mmol/L, Q_g = 10 mL/min, t = 90 s).

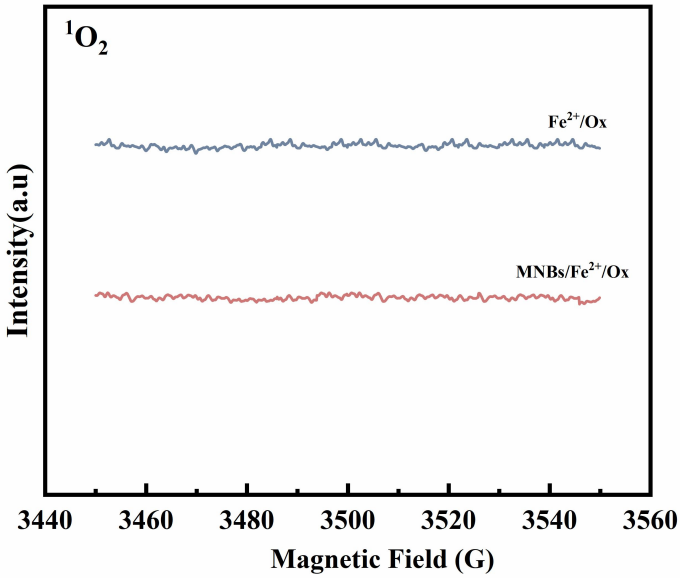

Fig. S5 TEMP spin trapping EPR spectra of $^1O_2$ in the system with and without MNBs participation. (pH = 7.0, [Fe^{2+}] = 0.1 mmol/L, [oxalate] = 0.5 mmol/L, Q_g = 10 mL/min, t = 90 s).

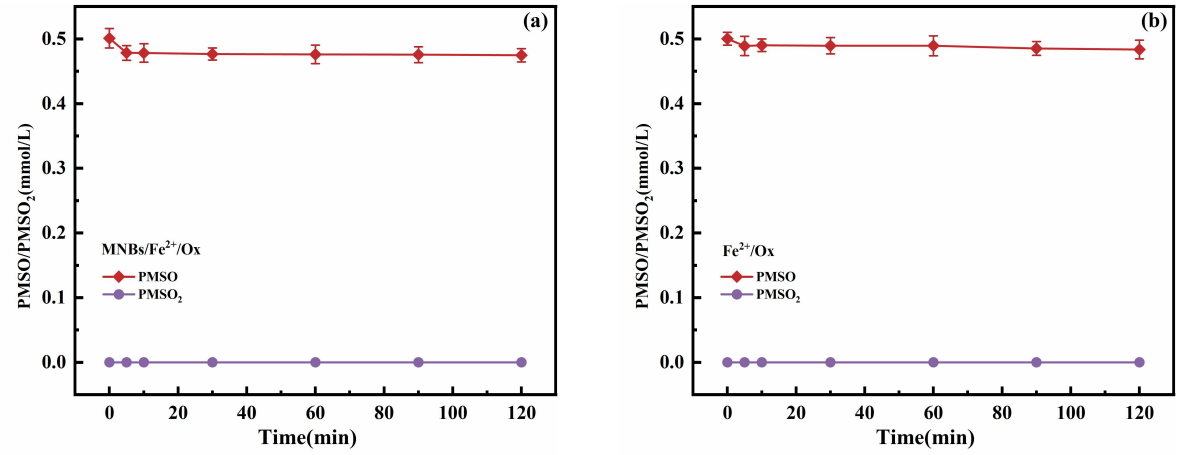

Fig. S6 Variation of PMSO and $PMSO_2$ content in the system with (a) and without (b) MNBs participation. (pH = 7.0, [Fe^{2+}] = 0.1 mmol/L, [oxalate] = 0.5 mmol/L [PMSO] = 0.5 mmol/L, Q_g = 10 mL/min, t = 90 s).

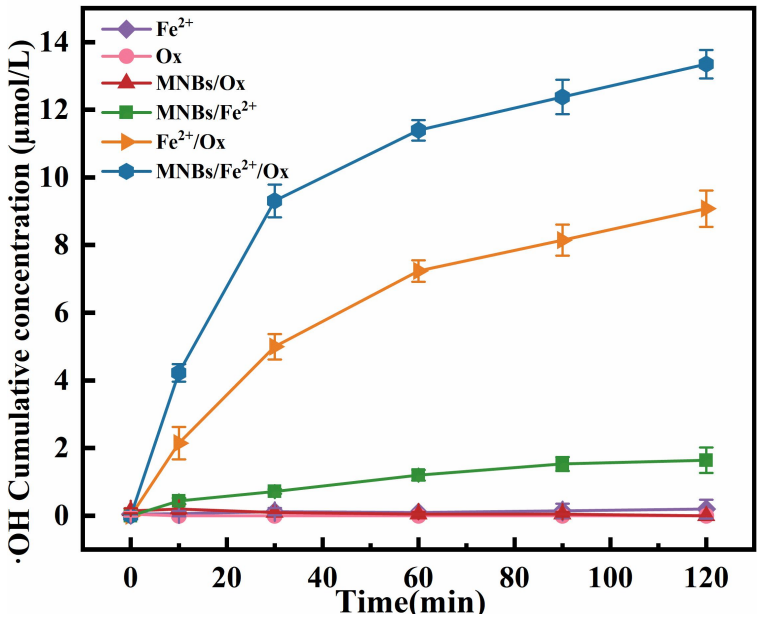

Fig. S7 The change of ·OH concentration under different system conditions. (pH = 7.0, [Fe^{2+}] = 0.1 mmol/L, [oxalate] = 0.5 mmol/L, Q_g = 10 mL/min, t = 90 s).

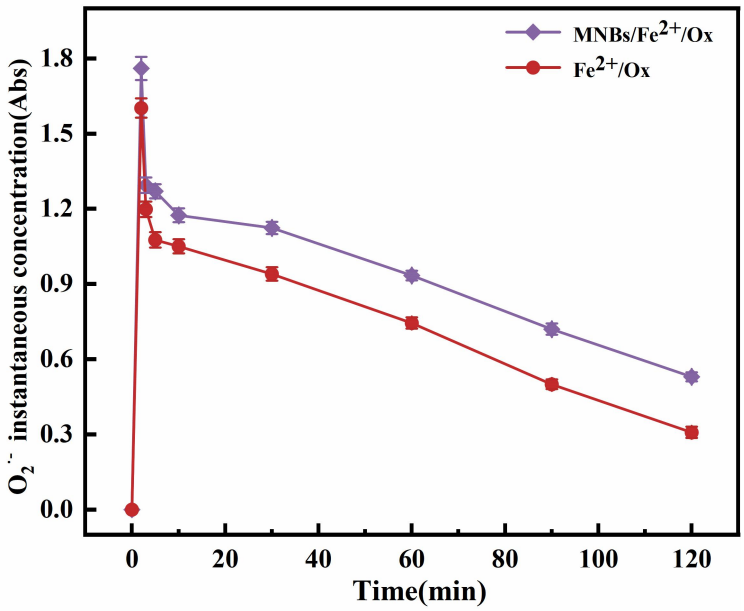

Fig. S8 The change of $O_2^{\bullet-}$ concentration in the system with and without MNBs participation. (pH = 7.0, [Fe^{2+}] = 0.1 mmol/L, [oxalate] = 0.5 mmol/L, [NBT] = 10 mmol/L, Q_g = 10 mL/min, t = 90 s).

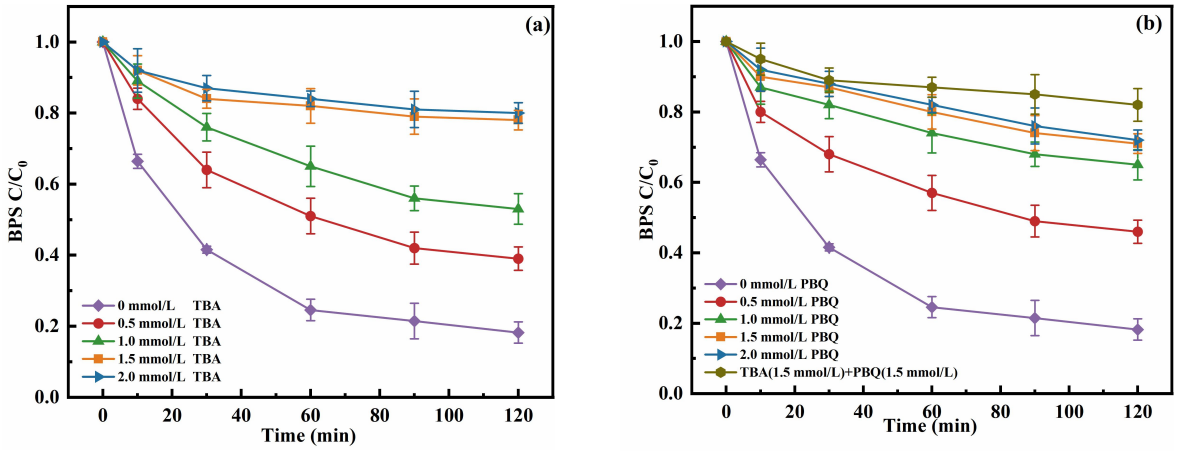

Fig. S9 Degradation curves of BPS at different scavenger concentrations: (a) TBA; (b) PBQ and TBA+PBQ. (pH = 7.0, $[Fe^{2+}]$ = 0.1 mmol/L, [oxalate] = 0.5 mmol/L, BPS = 100 μg/L, Q_g = 10 mL/min, t = 90 s).

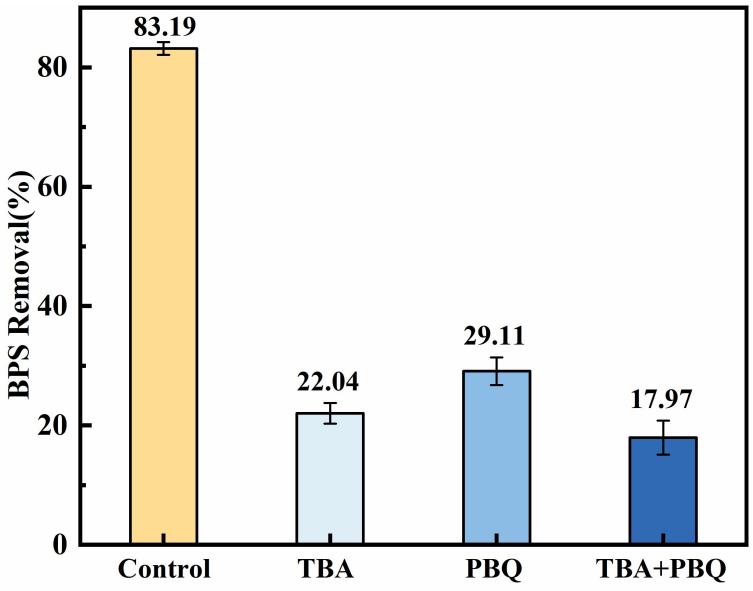

Fig. S10 Effect of radical scavengers on the degradation of BPS by the system. (pH = 7.0, $[Fe^{2+}]$ = 0.1 mmol/L, [oxalate] = 0.5 mmol/L, BPS = 100 μg/L, Q_g = 10 mL/min, t = 90 s, [TBA] = 1.5 mmol/L, [PBQ] = 1.5 mmol/L).

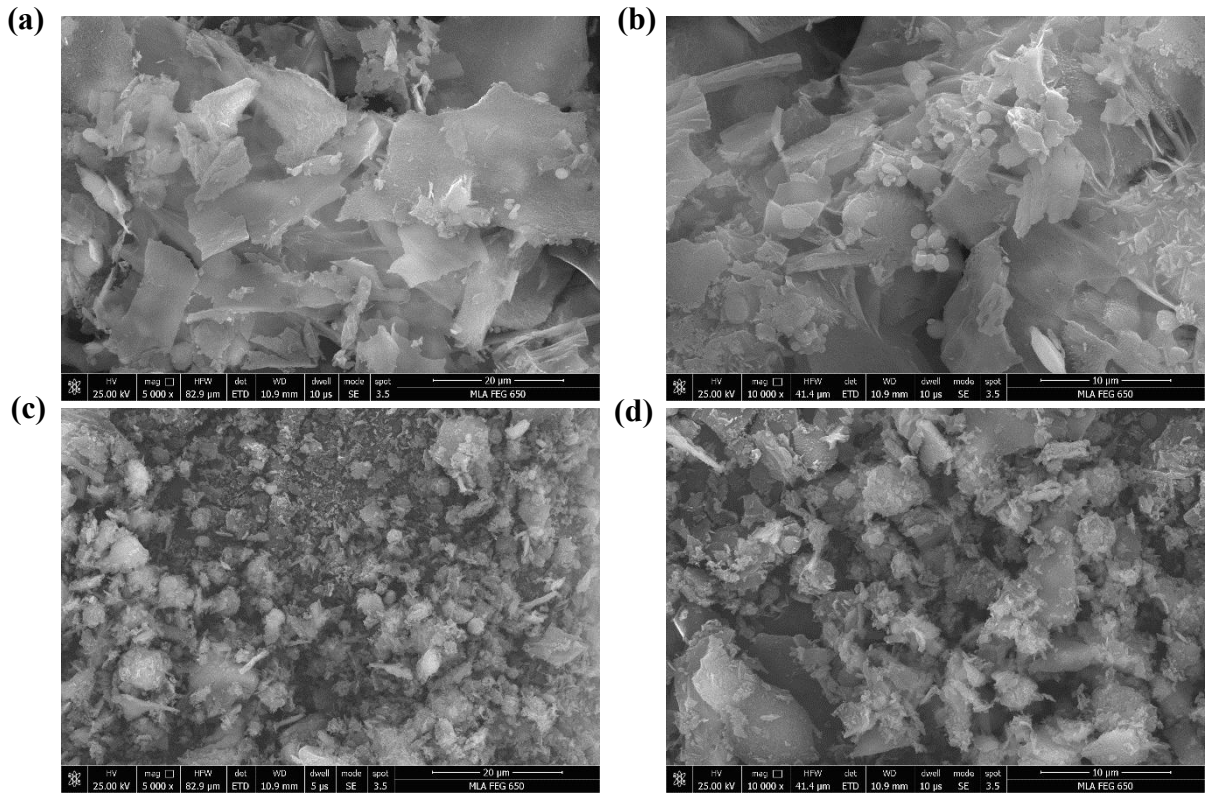

Fig. S11 SEM characterization of flocs: involvement of MNBs (a, b); no involvement of MNBs (c, d). (pH = 7.0, [Fe^{2+}] = 0.1 mmol/L, [oxalate] = 0.5 mmol/L, BPS = 100 μg/L, Q_g = 10 mL/min, t = 90 s).

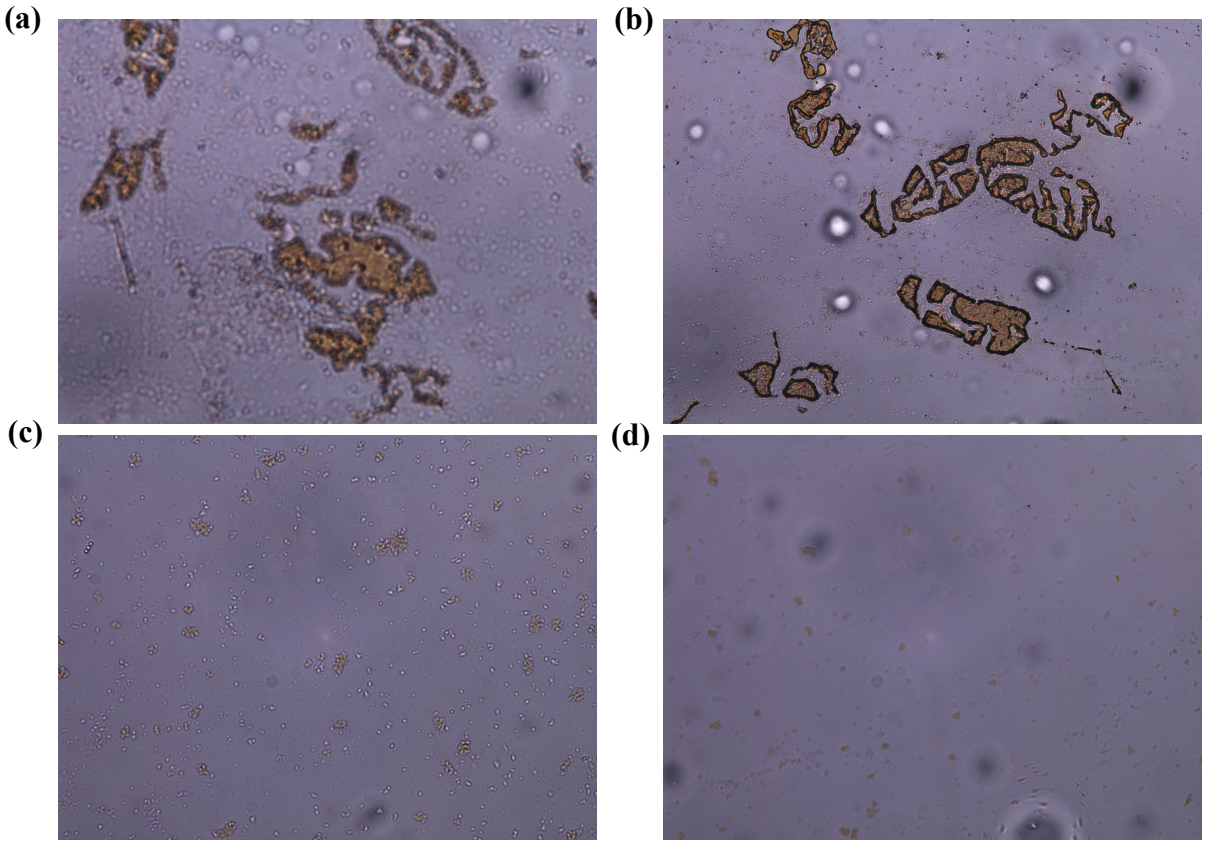

Fig. S12 Characterization of flocs shape: involvement of MNBs (a, b); no involvement of MNBs (c, d). (pH = 7.0, $[Fe^{2+}]$ = 0.1 mmol/L [oxalate] = 0.5 mmol/L, BPS = 100 μg/L, Q_g = 10 mL/min, t = 90 s).

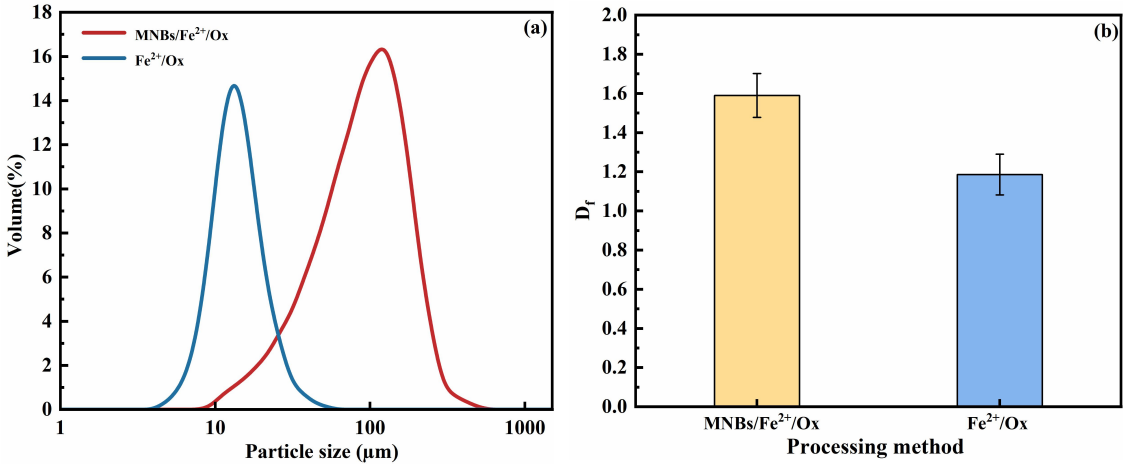

Fig. S13 Particle size distribution (a); floc fractal dimension (D_f) (b). (pH = 7.0, $[Fe^{2+}]$ = 0.1 mmol/L, [oxalate] = 0.5 mmol/L, BPS = 100 μg/L, Q_g = 10 mL/min, t = 90 s).

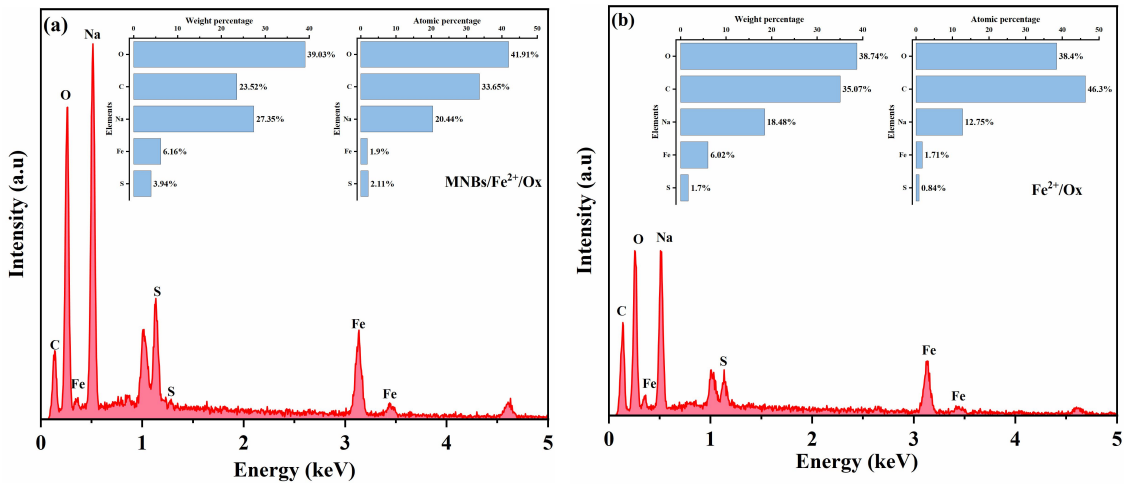

Fig. S14 EDS energy spectrum analysis: involvement of MNBs (a); no involvement of MNBs (b). (pH = 7.0, [Fe^{2+}] = 0.1 mmol/L, [oxalate] = 0.5 mmol/L, BPS = 100 μg/L, Q_g = 10 mL/min, t = 90 s).

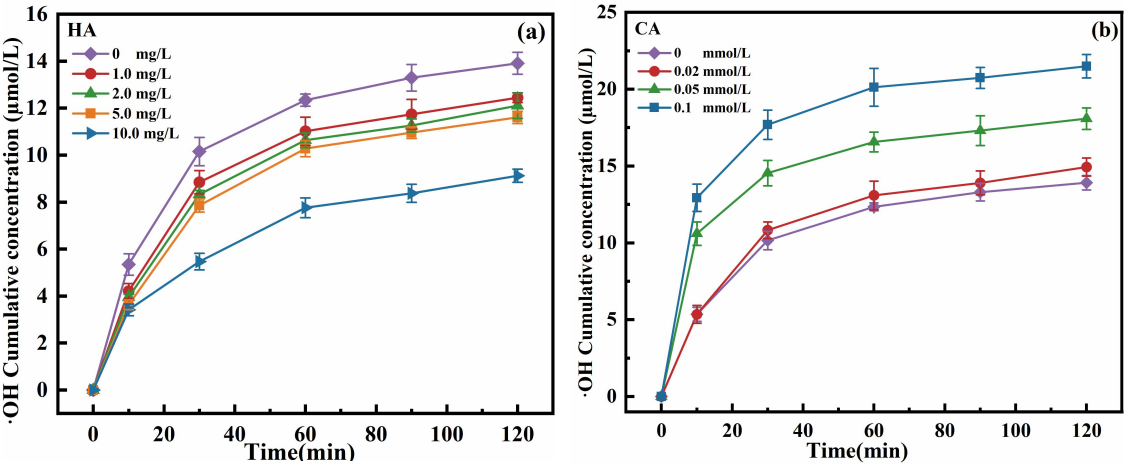

Fig. S15 Addition of HA (a) and CA (b) changes in ·OH concentration in the system. (pH = 7.0, [Fe^{2+}] = 0.1 mmol/L, [oxalate] = 0.5 mmol/L, Q_g = 10 mL/min, t = 90 s).